

Article

Pressure-Dependent Crystal Radii

Oliver Tschauner 

Department of Geoscience, University of Nevada Las Vegas, Las Vegas, NV 89154, USA;
oliver.tschauner@unlv.edu

Abstract: This article reports the pressure-dependent crystal radii of Mg, Si, Ge, Be, Fe, Ca, Sr, Ba, Al, Ti, Li, Na, K, Cs, and of some rare earths, that is: the major Earth mantle elements, important minor, and some trace elements. Pressure dependencies of O^{2-} , Cl^- , and Br^- are also reported. It is shown that all examined cation radii vary linearly with pressure. Cation radii obey strict correlations between ionic compressibilities and reference 0 GPa radii, thus reducing previous empirical rules of the influence of valence, ion size, and coordination to a simple formula. Both cation and anion radii are functions of nuclear charge number and a screening function which for anions varies with pressure, and for cations is pressure-independent. The pressure derivative of cation radii and of the anion radii at high pressure depends on electronegativity with power -1.76 .

Keywords: crystal radii; pressure-dependent ionic radii; high-pressure chemistry

1. Introduction

Solid state chemistry, geochemistry, cosmochemistry, and material science often recur to the concept of ionic radii in interpreting or predicting structures and reactions of condensed matter. Geo- and cosmochemistry rely on ionic radii in the interpretation of element abundances [1]. In material science and solid state chemistry ionic radii are used to define tolerance factors which correlate arrays of chemical composition with structure types (e.g., [2,3]). The concept of ionic radii is more than a convenient simplification: element abundances in rocks are the result of a multitude of chemical reactions and element redistributions between solid, liquid, and fluid state. Direction-dependent bonding is spatially averaged over this extensive series of element redistributions and it can be shown that ionic radii are a rather accurate representation of these net chemical processes. Despite their original definition [1], crystal and ionic radii are not classical approximations but represent the limiting case of spatial spherically symmetric averages of the valence electron states mapped into the configurational space (hence, there is no violation of orthonormality of states).

Despite the importance of the radii concept in geochemistry and despite the fact that pressures in Earth extend over 100 GPa in the mantle and to nearly 400 GPa in the inner core, the effect of pressure on the ionic and crystal radii has not been explored much. However, it is easy to see that this effect is not negligible: changes in pressure as they occur between the Earth's crust and core-mantle boundary are sufficient to change the chemical behavior of elements. For instance, the change in energy that occurs upon compressing mantle peridotite from the shallow lithosphere to the core mantle boundary over an interval of ~ 130 GPa of pressures is estimated to about 1.6 eV/at [4]. With an approximate bulk composition of Mg_2SiO_4 , three-quarters of the Earth's mantle is oxygen as constituent chemical species, and within this approximation the O^{2-} anion dominates the increase of the electronic inner energy induced in Earth material by compression. Between 0 and 136 GPa (the pressure of the core mantle boundary), the contraction of the crystal radius of O^{2-} in four- to six-fold coordination by Mg and Si is from 1.28 or $1.26 \cdot 10^{-12}$ m, respectively to $\sim 1.2210^{-12}$ m (see Section 3), hence: $4/3\pi \Delta r^3 \cdot 1.36 \cdot 10^{11} \text{ N/m}^2 = 2.50 \cdot 10^{-19} \text{ J/at} = 1.56 \text{ eV/at}$ (of O^{2-}). Differences between energy levels of bonding and anti-bonding electron states of ions in



Citation: Tschauner, O. Pressure-Dependent Crystal Radii. *Solids* 2023, 4, 235–253. <https://doi.org/10.3390/solids4030015>

Academic Editor: Sophie Guillemet-Fritsch

Received: 7 June 2023

Revised: 21 July 2023

Accepted: 26 July 2023

Published: 28 August 2023



Copyright: © 2023 by the author. Licensee MDPI, Basel, Switzerland. This article is an open access article distributed under the terms and conditions of the Creative Commons Attribution (CC BY) license (<https://creativecommons.org/licenses/by/4.0/>).

the crystal field of oxide anions are of comparable magnitude. Hence the pressure-induced increase in electronic energy is within a range that allows for formation of bond states different from those that we know from ambient pressure. This type of change defines proper high-pressure minerals [4,5].

Geochemical distribution patterns of igneous rocks are expected to reflect in part processes that occurred in source regions deep in the Earth's mantle. Hence, it is important to correct for the effect of pressure on the radii since they can change the element distribution in those deep source regions.

It is the purpose of this article to use an extensive set of available compression data to assess pressure-dependent radii of elements. Here, crystal radii rather than ionic radii are determined.

Prewitt and Downs [6] proposed a set of general trends for compression of cation-oxide bonds, in particular that (a) over a given pressure interval, longer bonds contract more strongly than shorter ones, (b) bonds become more covalent with decreasing bond length, and (c) the coordination number of a cation increases with pressure, which latter rule was already proposed by Shannon and Prewitt [7]. In both studies, it was stated that anions are more compressible than cations. More recently, these concepts were reexamined, confirmed, and extended to molecular solids by Grochala et al. [8] by means of concepts of theoretical chemistry and by relating them to a large set of experimental and computational studies that had been carried out since the publication of Prewitt and Downs' paper [6]. Gibbs et al. [9,10] have examined the effect of pressure on bonded radii by applying the Baader charge separation approach to electron density distributions obtained by density functional theory. Gibbs et al. [10] found linear dependences of these 'bonded radii' on pressure but also observed that bond distances are affected by the difference in electronegativity between cations and the oxide anion [9].

Cammi et al. [11] and Rahm et al. [12] calculated non-bonding radii of most elements between 0 and 300 GPa by using a mean-field approach. They reported discontinuous contractions of radii as result of valence changes from involving orbitals in the valence states that are empty at ambient pressure and from hybridization of inner shell electrons with the valence shell. Hence, pressure-induced changes in the configuration of the outer shell electrons cause marked electron density contractions which are expected to cause structural reconfigurations of their compounds as well as changes in their chemical behaviour. Tschauner [13] used empirical crystallographic data to determine pressure-dependent crystal radii of Mg, Si, and Ba in sixfold coordination by O^{2-} and found that these cation radii are not significantly dependent on individual structures. Hence, the concept of crystal radii appears to be valid over pressures of 10–100 GPa, at least for those ions. Further, within uncertainties, all three cations exhibited linear dependence on pressure. The O anion was found to exhibit initially a marked nonlinear compression converging towards weaker linear compression, consistent with the observations by Prewitt and Downs [6] that anions compress more strongly than cations. However, the potential coordination dependence of the O^{2-} anion radius was not examined in [13]. Tschauner and Ma [4] reported radii of K, Mg, Ca, Al, Si for different cation coordinations and explicitly considered the effect of coordination on the oxide anion radius. Tschauner and Ma [4] found that K, Mg, Ca, Al, Si exhibit linear contraction over the examined pressure intervals within uncertainties but with the exception of fourfold-coordinated Si. The heavier cations K and Ca are more compressible than the lighter ions Mg, Al, and Si. In addition, it was observed that the higher the cation valence, the lesser the pressure effect, again consistent with [6], whereas the available data did not support the general trend for the pressure dependence of crystal radii with bond coordination that was proposed in [6].

The results in [4,13] indicate that the concept of radii remains meaningful over the pressure range of 0–160 GPa; as at ambient pressure, the effect of bond polarizability [9] is averaged for sufficiently large sets of crystal data. Because of that, ionic radii and crystal radii are useful in explaining chemical substitution and correlations of structure types with composition. Based on [4,13], this is expected to hold for pressures at least up to 160 GPa.

Furthermore, a potential pressure-induced increase in covalency of bonds does not appear to devalidate the crystal radius because no marked deviations from linear compression of the cation radii for the given anion have been observed. The present study largely extends and generalizes this work by providing a set of pressure-dependent radii for thirty-five ions of twenty different chemical elements in various coordinations and valencies. O-anion radii for different coordinations by cations are used for assessing crystal radii from an extended number of structural analyses of compounds under compression. Moreover, the pressure-dependent radii of Cl^- and Br^- are assessed for six- and eightfold coordination in order to obtain comparative sets of cation radii from oxides and halogenides for alkaline elements (Table 1). It is found that cation crystal radii are rather independent of the difference in anion electron affinity and on individual structures within small differences. Furthermore, within uncertainties, all crystal radii contract linearly with pressure. The range of pressure dependencies is similar to that reported by Gibbs et al. [10] for Ca, Si, and La. Based on the present augmented set of pressure dependencies, general correlations of ionic compressibility and nuclear charge number of the radii and their pressure derivatives of the radii and electronegativity are established, and these correlations encompass the rules previously stated by Prewitt and Downs [6].

Discussion starts with evaluating the anion compression models, then each group of cations is briefly discussed. General results of the pressure effect on these radii, the relation between the radii and their pressure dependence with nuclear charge number, and with electronegativity, are presented in Section 4.

2. Methods

Crystal radii are determined from bonding interatomic distances as the linear combination of cat- and anion radii. Pauling [14], Shannon and Prewitt [15], and Shannon [16] have assessed crystal radii for ambient pressure. The present assessment of pressure-dependent radii relies on three principal criteria:

- (1) For given valence and bond coordination the assessed radii should be independent of the structures, therefore;
- (2) Radii should be assessed through different crystal structures, if available. Wherever possible cation radii are assessed through structures with different anions
- (3) Radii derived from structures with ions on general positions are given preference.

Structure data for high-pressure minerals at ambient pressure [5,17] cannot be used here because their bond distances represent the present state at ambient pressure but not at the conditions of formation. Many good experimental compression studies are on solid solutions such as bridgmanite-hiroseite, aluminous or ferraluminous bridgmanite, etc. These studies are very valuable in geophysics and petrology but of no immediate use here. Only compression and structure data of pure endmembers can be used to assess crystal radii. This constraint acts as a fourth, auxiliary criterion. Data obtained from specimens compressed in hydrostatic or nearly hydrostatic media and data from single crystal diffraction studies are given preference, wherever available. No peroxides or hydroxides were considered (with the single exception of $\text{Ba}(\text{OH})_2$ because the effect of the proton appears to be within the scatter of the data for this difficult cation see Section 3.2). Ambient-pressure radii were not fixed in the fits of radii compression, thus allowing for a comparison of the interpolated 1 bar radii with literature values that were taken from [16]. Unless stated differently, all data are for 300 K. In order to minimize the number of superscripts in text and figures, valences are specified only for multivalent ions and in case of ambiguity. For convenience, radii are given in Å, unless stated otherwise. The term coordination is used here in the sense of bond coordination. To avoid lengthy wording but also conflicts with the reference style, coordination is given as Roman numbers in square brackets. All radii presented in this study are crystal radii. Henceforth, the term radii shall be used for crystal radii and ionic radii shall be mentioned explicitly as such.

As already indicated, above crystal and ionic radii never establish an exact representation of chemically bonded atoms but the limiting case of valence configuration states

in spherically symmetric spatial average over a sufficiently large number of compounds. Consequently, deviations between radii obtained from compression data of different compounds are the largest source of uncertainty, whereas propagation of uncertainties from measured interatomic distances are much less significant. Radii obtained from small or from single sets of compression data are potentially subject to systematic uncertainties which will only become assessable through further compression studies in the future. The actual assessment of bond coordination is another potential source of systematic error. Here, in doubtful cases, the interpolation of pressure-dependent radii to ambient pressure is used to constrain bond coordination: in almost all such cases, the 1 bar radii match the radii listed by Shannon [16] within small uncertainties. Crystallographic data that were used in this study are referenced in Table 2.

3. Discussion

3.1. Anions

All three examined anions, O^{2-} , Cl^- , and Br^- , exhibit compressibilities that are nonlinear at low pressure but approach linear compression asymptotically with increasing pressures. This behaviour can be cast into the functional form $r = \text{const} \cdot P^{-m}$ (Table 1). In [13], an empirical equation was presented for the pressure effect on the O^{2-} anion in sixfold coordination. The equation was obtained from interatomic distances of Mg-O and Si-O in binary and ternary compounds with emphasis on high-pressure minerals. As a starting point for pressure-dependent crystal radii of O^{2-} [VI], the Baader radii of Si and O in compressed silica by Du and Tse [18] were used. The Baader radii at ambient pressure were corrected to match the crystal radii of Mg and Si in octahedral bond configuration. Then, the pressure dependence of O^{2-} [VI]—as computed in [18]—was corrected to yield a consistent set of structure-independent crystal radii for Mg and Si. This resulted in a relation $r(O^{2-}) = 1.269 \cdot P^{-0.0176}$, where P in GPa and r is the anion crystal radius in Å (Table 1). In the present paper, the set of oxide phases is much expanded (Table 2). The augmented set of crystal data requires a better assessment of the effect of O-anion coordination by cations (Table 1) than previously. Initially, only the constant term was varied to match the 1 bar radius of O^{2-} in each coordination. However, it was found that cation radii for some structures (eskolaite, ABO_3 -perovskites) exhibited slightly nonlinear or non-monotonous pressure dependencies. It was found that these nonlinearities vanish if the power of the O-anion compression s is modified for coordinations less than six (Table 1) and that the resulting cation radii r_c are structure-independent within uncertainties as defined by the variance of cation radii obtained from different phases.

Compression data of liebermannite [19] provide radii for K[VI]. These values were used to test K[VI] radii obtained from halogenide compression data [20–22]. Hereby, Cl and Br anion compression was initially set to be equal to that of O^{2-} [VI], then corrected as to obtain equal radii of Na[VI,VIII] and K[VI,VIII] from both chlorides and bromides and to match K[VI] from K-O bond distances. In a second step, the obtained Cl^- and Br^- radii were tested with CsCl, and CsBr [22]: correct anion radii should give equal radii of Cs[VIII] for both salts. This was found to be the case.

Table 1. Power and constant prefactors for $r(\text{anion}) = r_0 \cdot P^m$ (P in GPa). The physical meaning of the functional form of $r(\text{anion}, P)$ is discussed in Section 4.3.

Ion	M	r_0 [Å/GPa ^m]
O^{2-} [II,III]	−0.0040(2)	1.210(5)
O^{2-} [IV]	−0.0045(5)	1.238(3)
O^{2-} [VI]	−0.0176(2)	1.269(2)
Cl^- [VI]	-	$1.62 - 0.02 \cdot P^*$
Cl^- [VIII]	−0.07(1)	1.66(1)
Br^- [VIII]	−0.078(3)	1.85(2)

* Pressure range was too small to assess the power.

3.2. Alkaline and Alkaline Earths Elements

Radii of some alkaline earth ions have been assessed in two previous publications [4,13]. Hence, the discussion of the new results starts with this group of elements. The pressure-dependent crystal radii of Be[IV], Mg[VI,X], Ca[VI,VII,VIII,IX,X], Sr[VI], and Ba[VI,VIII] are assessed (Figure 1a,b). The previous results for Ba [13] have been reassessed by distinguishing compression for different anion bond coordination and Ba coordination which, in consequence of the generally high and compression-dependent coordination of Ba, give compressibilities with larger uncertainties than for Mg and Ca. This is owed in part to the difficulty in assessing O fractional coordinates from X-ray diffraction data of phases with a atoms of as large a form factor as Ba, in part from an intrinsic difficulty in assessing bond coordination for large cations in absence of actual electron density maps or EXAFS. Hence, the liberty was taken to disregard some of the crystal data that were used in the previous study [13]. As selection criterion, it was examined which data interpolate to established ambient pressure radii of Ba. The selected sets of data interpolate to Ba[VI–VII] and [VIII] at ambient conditions (Figure 1, right panel). This does not imply that all data that are disregarded here are incorrect, but a further splitting into intermediate coordinations is not within the frame of this study. The issue of uncertain bond coordination also avail for Sr. Interpolation of the pressure dependence of the radii to ambient pressure is consistent with a coordination of six (see Table 2). Previous data for Mg were augmented (Table 2) and the pressure dependence of Mg[X] that was reported in [13] was corrected for the O^{2-} coordination in bridgmanite. With this correction, Mg[X] exhibits a contraction that intersect the crystal radius of Mg in postperovskite-type $MgSiO_3$ at 116 and 120 GPa [23,24]. All alkaline earths compress linearly within uncertainties over the examined pressure range. Radii of Be[IV] were obtained from compression studies of bromellite (BeO , [25]). Compression studies on other Be-silicates and of chrysoberyl [26] exhibit much scatter around the values obtained from bromellite. Hence, the third criterion in Methods was applied here: to give preference to radii obtained from interatomic distances in structures without internal degrees of freedom in case of discrepancies with more complicated structures. Hence, only radii from bromellite were used to define the pressure dependence of Be[IV]. It is noted that Ca[VIII] from the high-pressure CsCl-type CaO phase interpolates to the ambient pressure radius Ca[VII] (based on Shannon 1976 [16]) and that Ca[X] in compressed synthetic davemaoite [27] interpolates to Ca[IX] at ambient pressure (Table 2). This observation has been made already by Tschauner and Ma [4] and an interpretation is presented here in the Results.

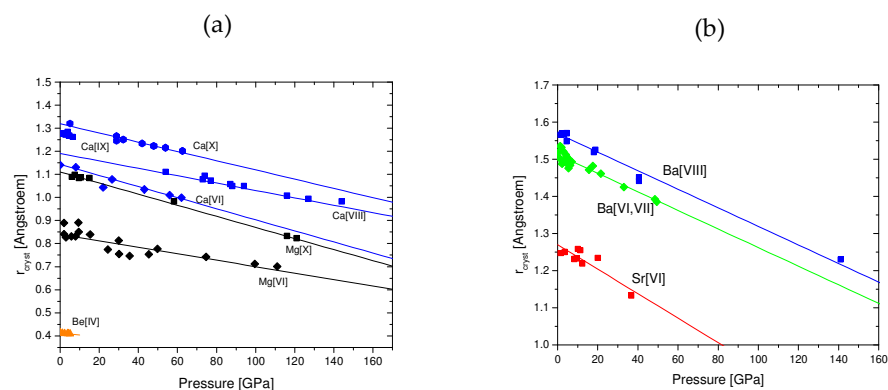


Figure 1. Pressure-dependent crystal radii of the examined alkaline earth ions. (a) Be, Mg, Ca. (b) Sr and Ba. Coordination is given in square brackets. For all ions, compression is negative and linear within uncertainties. Lines show the least-square fits of the compression (see Table 2).

Crystal radii of Li, Na, K, and Cs were obtained for different bond coordinations (Figure 2, Table 2). Radii were derived from cation-oxide, -chloride, and -bromide bonds for Na, K, and Cs, and from cation-oxide bonds for Li. Radii obtained from cation-oxide distances exhibit overall linear compression (Figure 2, filled symbols). However radii

obtained from halogenides show crossover to different linear compression regimes upon compression (Figure 2, hollow symbols). Ambient-pressure radii interpolated from those high-pressure regimes match established ambient pressure crystal radii [16] and are specified as such (Table 2). The possible causes of these pressure-induced changes are discussed in Section 4. The fact that the same crossover -is observed for different halogenides of the same cations suggests that it -is not an artifact of an insufficiently accounted pressure dependence of the anion radii, although this cannot be fully excluded with such limited data. Generally, the shift towards higher coordination with pressure -is well along the lines of the rules observed by Prewitt and Downs [6] and Grochala et al. [8]. Na[VII] from albite compression data exhibits- large scatter and probably reflects changing bond coordination upon compression.

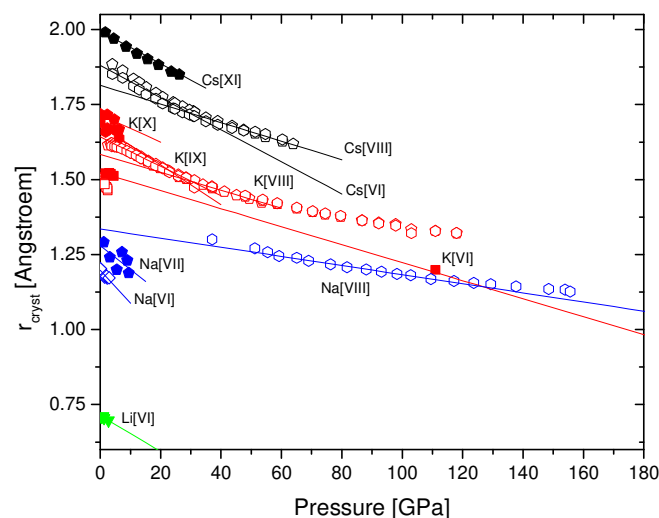


Figure 2. Crystal radii of Li, Na, K, and Cs, bond coordinations given in square brackets. Filled symbols represent data from cation-oxide distances, hollow symbols = radii from cation-chloride and -bromide distances, respectively. Fitted pressure dependences are shown as lines and are given in Table 2. There is a change in compressibility of K[VIII] between 60 and 70 GPa such that the high-pressure regime interpolates to K[VI] at 0 GPa (see Section 4). The intersections of K[IX] and K[VIII] around 30–40 GPa and of K[VI] and Na[VIII] around 110–130 GPa are noteworthy.

3.3. Rare Earths

Rare earth elements, that is, Sc, Y, and the lanthanides, are pivotal in mantle geochemistry and are components in many materials of high interest in solid state physics and material science. The compression behaviour and phase transformation sequences of sesquioxides of rare earths have been studied, but in particular for the lanthanide oxides fractional atomic coordinates of O are not considered sufficiently accurate for obtaining crystal radii, because of the large difference between the form factors of O and the lanthanide ions. None of those studies was conducted under hydrostatic or nearly hydrostatic pressure; the reported bulk moduli vary largely, probably reflecting deviatoric stresses and overlap of oxide and hydroxide diffraction signal as unresolved parameters. Therefore, cell shapes and reported interatomic distances are also likely to be compromised. Consequently, these data were omitted here and only data from the single crystal compressions studies of the aluminates of Sc, Y, La, Pr, and Gd were used to derive crystal radii to between 8 and 10 GPa [28–32]. Within this pressure range, all radii contract linearly with pressure (Figure 3, right side) and the dr/dP of La is within uncertainty equal to those reported by Gibbs et al. [10], while the contraction of Y is found to be slightly larger than those calculated in [10]. The radii of Al were compared with those obtained from corundum and found to match (Figure 3b). The radius of Sc [X] interpolated to 1 bar is somewhat larger than the radius reported by Shannon (1976, [16]). This suggests that this radius may exhibit

more variance than suggested by the present set of data derived from compression data of a single compound.

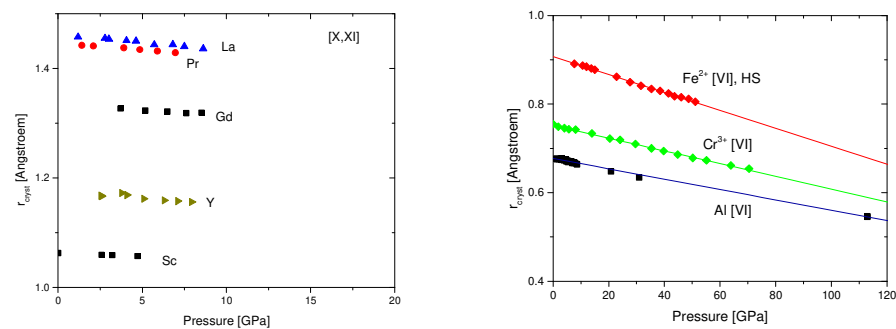


Figure 3. (Left): Radii of rare earth elements. (Right): Radii of Al, Fe^{2+} , and Cr^{3+} , all three in sixfold coordination. Fitted pressure dependences are shown as lines and are given in Table 2.

3.4. Al, Cr, Fe

Crystal radii of Al[VI] were obtained from three independent studies of corundum [33–35], chrysoberyl [26], and from four studies of aluminate perovskites [28–32] and its linear compression is therefore very well constrained up to nearly 120 GPa. The dr/dP of Al [VI] is almost identical with that calculated by Gibbs et al. [10]. Radii of Cr^{3+} [VI] were obtained from a single compression study of eskolaite [36]. Compression is linear.

Fe poses a particular problem because the radii of Fe^{2+} and Fe^{3+} (and higher oxidation states) are affected not only by coordination and valence but also by the valence electron spin state [16]. Moreover, valence electronic states of Fe are often mixed because of charge transfer between different sites. Mixed states along certain bond directions also affect bond distances and coordination. Charge transfer and spin state may change with pressure. Charge transfer blurs the bond coordination (and accounts for the large variety of pure iron oxides phases of different stoichiometry that occur at high pressure). Consequently, the large number of compression studies and structure analyses of compounds of Fe_xO_y yields a large scatter of apparent radii which cannot be corrected for the electronic effects mentioned above without ad hoc assumptions about spin states and charge transfer. Instead, only single crystal compression data for wuestite [37] were used to obtain radii for Fe^{2+} in the high spin (HS) state to 50 GPa. No robust data of Fe^{3+} could be obtained because not even hematite keeps a fixed spin state over a sufficiently large range of pressure (because of the Morin transition).

3.5. Si, Ge, Ti

The pressure dependence of Si^{4+} in [VI]-coordination was studied in [13]. Tschauner and Ma [4] provide an augmented set of data for Si[VI] and for Si[IV]. Pressure-dependent radii of Ti^{4+} were obtained from compression data of rutile, perovskite, and geikielite (see Table 2). Compression data of ilmenite in the literature show much variance, probably as result of a minor component of hematite in the examined specimens, and are not used here. Both Si [VI] and Ti^{4+} [VI] exhibit linear compression (see Figure 4).

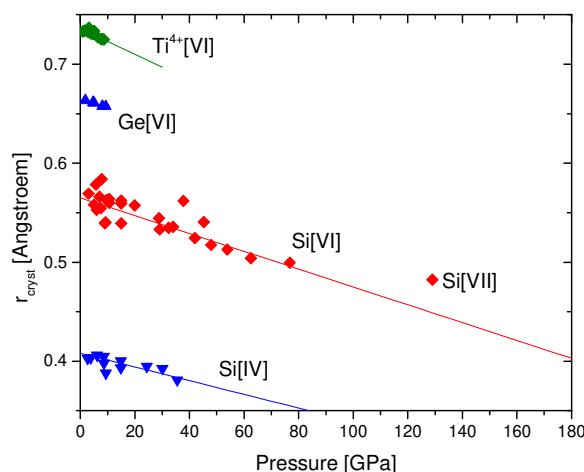


Figure 4. Crystal radii of the tetravalent cations Si, Ge, and Ti. Coordinations given in square brackets. Lines represent the fitted pressure dependencies.

Radii of Si[IV] from compression studies of ahrensite [38] and ferrous wadsleyite [39] show the same pressure dependence as pure silica and low-pressure silicate phases. However, the absolute radii are systematically shifted to higher values. Therefore, the interatomic distances were crosschecked for the spinel ahrensite by calculating the unit cell parameter [40] and were found to be systematically higher than the measured values. The same effect, though much less pronounced, has been found as a small offset of the u -parameter in the natural type ahrensite [41]. It is suspected that these examined high-pressure silicates exhibited hidden structural disorder (such as from partial oxidation of iron) and the data were not used here. In Tschauner and Ma [4], these data were used and this resulted in an apparent expansion of Si[IV] with pressure. Based on the point above, this apparent expansion is an artifact. The compression of Si[IV] as reported in Table 2 follows precisely the general correlation of radii and their pressure dependencies (see Section 4). Radii of Ge[VI] were obtained from a compression study of MgGeO_3 [42].

Table 2. Pressure dependencies of crystal radii r , interpolated ambient pressure radii r_0 , reference crystal radii r_{cryst} at 1 bar from reference [15], R^2 of the fitted pressure dependencies, and references to the studies whose structure data were used to obtain interatomic distances.

Element, [Coordination]	$-dr/dP$ [Å/GPa]	r_0 [Å]	r_{cryst} [Å] (Shannon 1976)	R^2	Ref.
Li[IV]	0.006(1)	0.713(1)	0.73	0.90	[43]
Na[VI]	0.0110(2)	1.198(3)	1.16	0.85	[21]
Na[VII]	0.008(4)	1.28(3)	1.26	0.32	[44]
Na[VIII]	0.00152(4)	1.335(3)	1.32	0.99	[21]
K[VI]	0.0030(3)	1.528(1)	1.52	0.98	[19,20,45]
K[VII] *	0.0030(1)	1.584(3)	1.6	0.99	[20]
K[VIII]	0.0049(1)	1.642(2)	1.65	0.99	[20]
K[VIII'] **	0.0014(1)	1.53(1)	1.52[VI]	0.97	[20]
K[IX]	0.0066(24)	1.68(1)	1.69	0.63	[46]
Cs[VI] *	0.0026(5)	1.79(4)	1.81	0.98	[22]
Cs[VIII]	0.0053(2)	1.88(1)	1.88	0.99	[22]
Cs[XI]	0.0057(2)	1.994(3)	1.99	0.99	[47]
Be[IV]	0.0010(2)	0.414(1)	0.41	0.76	[25]
Mg[VI]	0.0014(2)	0.84(1)	0.86	0.76	[4,13,48,49]
Mg[X]	0.0024(1)	1.11(3)	-	0.99	[4,23,24,50–52]
Ca[VI]	0.0024(1)	1.143(4)	1.14	0.99	[53]
Ca[VII,VIII] *	0.0016(1)	1.19(1)	1.2[VII]	0.97	[53]
Ca[VIII]	0.0034(2)	1.28(1)	1.26	0.98	[53]
Ca[IX,X]	0.0020(2)	1.319(8)	1.32[IX]	0.94	[26,54,55]
Sr[VI]	0.0033(6)	1.27(1)	1.32	0.77	[56–59]
Ba[VI,VII] *	0.0025(2)	1.512(4)	1.52[VII]	0.88	[60–65]

Table 2. Cont.

Element, [Coordination]	$-dr/dP$ [Å/GPa]	r_o [Å]	r_{cryst} [Å] (Shannon 1976)	R^2	Ref.
Ba[VIII]	0.0025(1)	1.569(4)	1.56	0.98	[60–65]
Sc[X]	0.00141(2)	1.032(1)	-	0.99	[29]
Y[X]	0.0025(6)	1.176(3)	1.215[IX]	0.71	[28]
La[XI,XII]	0.0030(2)	1.463(1)	1.4[X], 1.5[XII]	0.97	[30]
Pr ³⁺ [XI,XII]	0.0024(1)	1.446(1)	-	0.98	[31]
Gd[X]	0.0017(3)	1.332(2)	1.33[X]	0.86	[32]
Ti ⁴⁺ [VI]	0.0016(2)	0.746(8)	0.745	0.95	[42,54,65]
Cr ³⁺ [VI]	0.00144(2)	0.752(1)	0.755	0.99	[36]
Fe ²⁺ [VI,HS]	0.00202(3)	0.907(1)	0.92	0.99	[37]
Al[VI]	0.00117(2)	0.677(1)	0.675	0.99	[26,28–35]
Ge[VI]	0.00085(7)	0.665(1)	0.67	0.97	[42]
Si[IV]	0.00069(8)	0.408(2)	0.4	0.88	[48,49,66–69]
Si[VI]	0.0009(1)	0.565(2)	0.54	0.79	[4,13,23,24,27,42,50–52,70–74]

*: Interpolated from high-pressure interionic distances. See Discussion about the origin of these offsets between low- and high-pressure coordinations. ** This radius and pressure dependence are from data of KCl and KBr above 70 GPa and they interpolate to the ambient pressure radius of K[VI]. This observation is explained in Results.

4. Results

4.1. Pressure-Induced Structure Changes and Pressure-Dependent Radii

In advance of discussing the general aspects of the pressure-dependent radii, it is useful to look at the relation between structure types that are favoured by pressure and the pressure-induced changes in crystal radii. One merit of the ionic radii concept is with the simple but quite reliable prediction of structures for solid compounds [2,3]. In [5], it has been suggested that high-pressure polymorphs can be defined through the fact that they plot outside the fields of occurrence of their structure types, as defined by ratios of radii or, more quantitatively, by tolerance factors of their ionic radii at ambient pressure. For instance, for oxides ABO_3 in a correlation of the cation ratios r_A/r_B or of the ratio r_B/r_O versus the tolerance factor $t = (r_A + r_O)/[\sqrt{2} \cdot (r_B + r_O)]$ [3], the minerals enstatite, $MgSiO_3$, and wollastonite, $CaSiO_3$, plot far outside the range of perovskite structures [5]. Hence, this discrepancy in combination with the occurrence of high-pressure polymorphs such as perovskite-type Mg and Ca silicates was suggested to serve as an indicator for marked pressure-induced changes in the chemical bonds between the constituent atomic species [5]. If this concept is correct, the pressure-induced changes of cat- and anion radii are expected to shift the high-pressure polymorphs into the field of tolerance of their structures. This is the case, indeed, and it is illustrated here for perovskite-type oxides as a particularly large and well examined class of materials [3].

With the crystal radii of Si[VI], Mg[X], and Ca[X], the ratio r_A/r_B shifts $MgSiO_3$ and $CaSiO_3$ just into the perovskite field of oxides in a simple correlation of r_A and r_B (see [5]). However, this correlation neglects the influence of the oxide anion. Li et al. [3] have shown that at ambient pressure, a correlation between the tolerance factor t and the octahedral factor $o = r_B/r_O$ provides a much better means of predicting perovskite structures. With the pressure-dependent radii from Table 2, the octahedral factor o for bridgmanite and for davemaoite ranges between 0.444 and 0.456 and t is below 0.919 and 1.00, respectively. This relation of o and t holds to about 100 GPa where o drops below the lower bound of the perovskite field. This range of pressure is close to the transformation of bridgmanite to the postperovskite phase [23,24]. However, it is noted that $CaSiO_3$ remains in the perovskite structure despite $o < 0.4$. For octahedrally coordinated Si and O, and tenfold coordinated Mg, the parameters t and o remain within the perovskite field even at ambient pressure. This observation tentatively explains the metastability of bridgmanite: if t and o are far outside this range, a spontaneous collapse of the structure is expected. This is the case for the stable electronic configurations that correspond to the radii of Si[IV] and Mg[VI]. Hence, the transition from the metastable to the stable valence electron configuration in decompressed bridgmanite is sterically hindered (see Section 9 in Grochala et al. [8]) but the energetic barrier is low. Davemaoite, with a t around unity, is close to the upper limit in

t of the perovskite field and may need chemical substitution to survive at low pressures [75]. FeTiO₃ remains at the border between the fields of ilmenite and perovskite structures, crossing into the latter around 7–10 GPa, which is slightly below the 10–12 GPa of the phase boundary interpolated to 300 K. These borderline values of o and t are consistent with the existence of a metastable LiNbO₃-type phase of FeTiO₃: wangdaodeite [4]. However, with O²⁻ in fourfold coordination, the octahedral factor o for ilmenite and wangdaodeite drops below that of liuite around 6.5 GPa and this is a potential indicator for the stabilization of the perovskite- over the ilmenite- and LiNbO₃-type structures above that pressure. The fact that above 9–10 GPa, and along with further increase in pressure, o and t do not shift further into the perovskite field, is consistent with the observed breakdown of this phase to cottunite-type TiO₂ and FeO at high pressure [5]: the perovskite structure does not gain in stability with increasing pressure and is replaced by simple oxides once a denser arrangement of Ti in a titania phase becomes energetically favourable. Thermal contributions as well as reaction kinetics influence the actual pressure where breakdown of liuite is observed. Charge transfer and changes in the spin state of Fe are expected to influence the effective radius of iron but appear to have no decisive effect in this particular case since the pressure-dependent parameters o and t are overall consistent with the observed phase transformations in FeTiO₃.

4.2. General Considerations: Cations

The compression of cations is discussed first. All cation radii exhibit linear compression (Table 2). The range of cation radii contraction dr/dP of between $7 \cdot 10^{-4}$ to $7 \cdot 10^{-3}$ Å/GPa extends further but is overall comparable to the range of values previously assessed for Ca, Y, La, and Al ($9 \cdot 10^{-4}$ to $5 \cdot 10^{-3}$ [10], and for those elements the present study and the earlier work agree within uncertainties). However, the conclusion by those authors that crystal and ionic radii may be considered as basically incompressible within the range of pressures in Earth cannot be supported here in that generality. For instance, the radii of Cs[VIII,XI] and K[VIII,IX] decrease by ~30% between 0 and 100 GPa (Table 2, Figure 2). Moreover, the differences in radii contraction extend over one order of magnitude and such large relative differences, although across overall small values of compression, have potential impact on element partitioning over the range of the Earth mantle. Generally, the pressure dependence of crystal radii follows a simple systematics that extends from the more compressible alkaline cations and the anions to rather incompressible ions like Si, Ge, and Mg. The correlation between dr/dP and r_0 , the crystal radius of the ions at reference ambient conditions, is shown in Figure 5 (left panel).

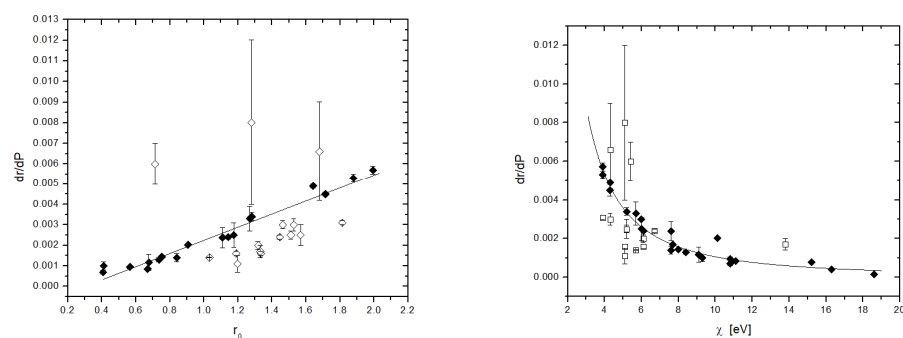


Figure 5. Overview and systematics of the pressure dependencies of the examined ions: correlation between $-dr/dP$ in 1/GPa and ambient pressure crystal radii r_0 in Å. **(Left side):** dr/dP as function of r_0 . Fit through filled symbol data, hollow symbols are for the following ions: Li[IV], Na[VI], Na[VII] Na[VIII], Cs[VI], Ca[VIII], [X], Ba[VI], [VIII], La, Pr, Gd. Filled symbols are for all other ions that represent the ‘mail trend’ (as explained in Section 4.2). **(Right side):** dr/dP as function of electronegativity χ in eV, at 0 GPa [76]. The fits are for the data that are represented as filled symbols; the same is true for the left panel.

All elements that deviate from the correlation $\text{const} \cdot \chi^{-1.75} = dr/dP$ also deviate from the linear correlation $dr/dp = 0.00329(15) \cdot r - 0.0010(2)$ (Equation (2)). The deviations indicate coordinations of ions whose electronegativity is smaller (Li[IV], Na[VII], K[IX]) or higher than those along the general trend and accordingly higher or smaller dr/dP . Note that each of the deviating ions occurs in a coordination which falls onto the correlation between dr/dP and r and χ , respectively. Thus, it is not the chemical species but specific coordinations of ions that exhibit excess compressibility (see Sections 4.1 and 4.2). The three data points for $\chi > 15$ eV represent the high-pressure dr/dP of the anions O, Cl, Br (see Section 4.3). The ions represented with filled symbols in Figure 5 give a linear correlation.

$$dr/dp = 0.00329(1) \cdot r - 0.0010(2) \quad (1)$$

with $R^2 = 0.96$. However, a good number of ions have been excluded from this fit (hollow symbols, a fit for all data gives a slope of 0.0029(4) and the same constant 0.0010(5) but with $R^2 = 0.66$) and this requires an explanation.

Generally, the finding agrees with the earlier proposition by Prewitt and Downs [6] that larger ions are more compressible than smaller ones. However, two aspects in this fit come to immediate attention: (1) Li[IV] and, potentially, though with large uncertainties Na[VII] and K[IX], are above the general trend; and (2) for radii $r > 1 \text{ \AA}$ a group of elements is below the correlation of Equation (1): Na[VI], Na[VIII], Cs[VI], Ca[VIII], [X], Ba[VI], [VIII], and Sc, Pr, and Gd in coordination [X–XI].

That large number of ‘exceptions’ raises the question if the restricted correlation for the remaining ions is at all meaningful. It may define with low-fitting correlation ($R^2 = 0.66$) marked variations that are due to specific reasons for each ion or may better be replaced by upper and lower bounds.

However, the deviations from (1) have a common, simple reason: Figure 5, right panel, shows the correlation of dr/dP and the electronegativity χ as a spatial average of valence electron binding energies. $\chi = \sum n_i e_i / n$ (sum running from $i = 1$ to n), n_i the occupation of the i th energy level e_i and n the total number of electrons [76]. Ambient pressure electronegativities by Rahm et al. [76] are used here. The same elements that exhibit a very strong linear correlation between dr/dP and r_0 also show a very strong correlation ($R^2 = 0.98$) with χ :

$$dr/dP = 0.061(14) \cdot \frac{1}{\chi^{1.76}} \quad (2)$$

and the power has an uncertainty 1.76 ± 0.15 . The same ions that deviate from (1) also deviate from (2) and this common behaviour explains the deviations: Ions with coordinations that are more compressible than those of the main trend, namely the ions Li[IV], Na[VII], K[IX], would require smaller electronegativity to match the main trend, whereas ions which are less compressible than those along the main trend (Na[VI], Na[VIII], Cs[VI], Ca[VIII], [X], Ba[VI], [VIII], Sc, Pr, and Gd) would require higher electronegativity to fall onto the trend. This indicates that relative to the main trend that is defined by Equations (1) and (2), the electron-electron repulsion of ions with positive excess compressibility is reduced, whereas that of ions with negative excess compressibility is enhanced. For Li[IV], a more pronounced internuclear repulsion possibly contributes to the offset relative to the main trend.

Hereby, it is essential that each of the elements which occur as ions in coordination that deviate from the main trend also occur in a coordination that falls right onto the main trend of correlations between dr/dP and r and χ , respectively: these are the ions represented by filled symbols in Figure 5. For instance, K[VIII] and [XI], Cs[VIII] and [XI] are obeying the relations given in Equations (1) and (2), but K[IX] and Cs[VI] deviate. Hence, it is not the chemical element but specific coordinations of ions of some elements which exhibit positive or negative excess compressibility. In other words, χ , as it is defined in [76], does not reflect differences in electronic state distribution that are specific for coordination, but

dr/dP does. However, for most ions and coordinations, there are no coordination-specific differences. These ions define the main trend in Equations (1) and (2).

This point of coordination-specific changes of dr/dP is further elucidated by looking at radii and their pressure derivatives from the perspective of electron screening functions. Before this is discussed, it is worth reporting the separate fit for the elements Na[VI], Na[VIII], Cs[VI], Ca[VIII], [X], Ba[VI], [VIII], Sc, Pr, and Gd[X–XI], because they obey a separate linear correlation between radius and dr/dP :

$$dr/dp = 0.00286(52) \cdot r - 0.0018(7) \quad (3)$$

with $R^2 = 0.98$. The merit of this separate fitting is discussed in Section 4.4. First, the overall linear correlation of the main trend in Equation (1) is discussed. The ionic compressibility is defined here as $(r_0)^{-3} (dr^3/dP)_T$ and with $dr^3/dP = 3r^2 dr/dP$, and with substitution of Equation (1) into this formula one obtains:

$$\begin{aligned} (dr^3/dP)_T &= 3(A \cdot r_0^3 - B \cdot r_0^2) \\ \Rightarrow (r_0)^{-3} (dr^3/dP)_T &= 3(A - B/r_0) \end{aligned} \quad (4)$$

where $A = 0.00329(1)$ and $B = 0.0010(2)$. In other words, for the main trend ions, the ionic compressibility is to first order a constant. dr^3/dP converges to zero for vanishing radii. B/r is a second order correction term and explains the minor deviation of the very small ions Be[IV] and Si[IV] from the main trend. Constant $3A$ has the dimension of a compressibility with value $9.8(1) \cdot 10^{-12} \text{ m}^2/\text{N} = 9.8(1) \cdot 10^{-3} / \text{GPa}$, which quantifies the change of ionic compressibility with increasing radius; that is, the change in compressibility with addition of further outer electrons for given principal quantum number L (because the radii vary periodically as a function of L and Z , see for instance [14]). This brings back the issue of the correlation between dr/dP and electronegativity and the causes of the deviations of ions in some coordinations from the rather strict general trends of Equations (1) and (2).

Following Pauling [14,77], the ionic radii are related to Z as $r = C/(Z - S)$ with C and S , a screening term that is a function of azimuthal and principal quantum numbers [77–79]. Consequently,

$$dr/dp = 0.00329(1) \cdot r - 0.0010(2) = A C/(Z - S) - B \quad (5)$$

Figure 6 shows that this is the case, indeed. In Figure 6, the ionic compressibility has been rescaled as $\beta = (r_B)^{-3} (dr^3/dP)_T$ with r_B the Bohr radius. β is given in $1/\text{GPa}$ and this somewhat unusual measure of ion compression describes the compressibility of the ions as multi-electron systems relative to the reference volume of a single electron, as defined by the Bohr radius r_B , whereas the proper ionic compressibility $(r_0)^{-3} (dr^3/dP)_T$ is invariant of Z or any other atomic parameter within uncertainties (Equation (4)). β is illustrative in showing the relation between ion compression and nuclear charge number Z . The relation between dr/dP and Z shows an equivalent systematics. It is given below in Section 4.4.

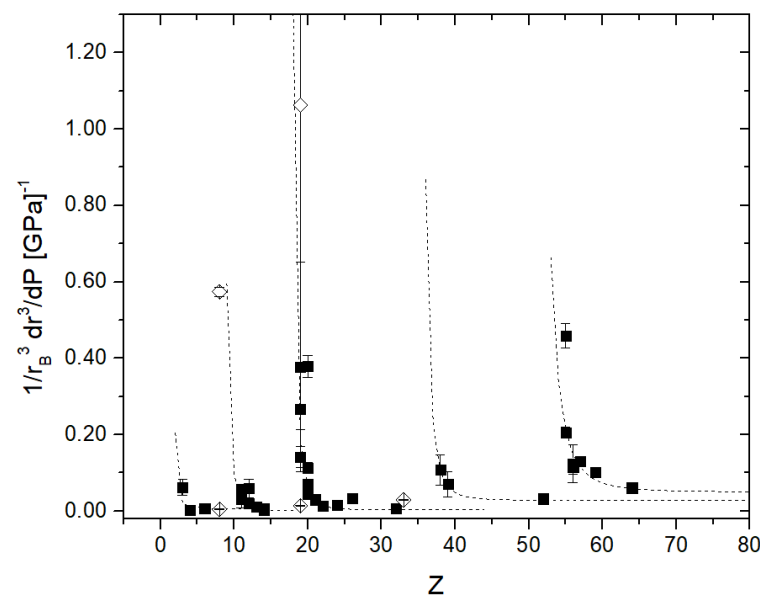


Figure 6. Ionic compressibility as a function of the nuclear charge number Z . The correlation is equivalent to that of the ionic radii and Z (see [14,77]) and determines the pressure-induced changes in the outer electron configurations of the ions. Compressibilities of cations are given in Table 2 shown as black squares; initial and asymptotic high-pressure compressibilities of the anions are shown as hollow diamonds (see Section 4.3).

The relation between β and Z is periodic along the periodic table, similar to that of the radii and Z [14,77–79] and this is expected, based on Equations (1), (4) and (5): for elements of given principal quantum number L , the ionic compressibilities β decrease with increasing number of electrons in the valence shell of the ions. This is not unexpected because a higher density of electrons in the valence shell increases repulsion through their Coulomb and exchange interactions and, therefore, resistance to compression. Thus, the observed dependence of β on Z shows that β reflects the mutual repulsion of the electrons. Alkaline and alkaline earths are the most compressible ions, whereas cations with filled p - and d -states are the less compressible the higher the filling of these orbital states. In second order, a more effective screening with increasing electron density and the availability of a larger set of orbital states, for both elements from rows $L \geq 4$ and for ions in higher coordination, increase compressibility. Hence, row $L = 2$ ions with filled p -states should be the least compressible and this is observed. For illustration, a ‘crystal radius’ of C^{4+} [IV] has been obtained from the bond distances of diamond under compression [80]: considering that a spherical average of valence electron distributions is not expected to be a good match for the highly covalent bond of diamond, the extremely low compressibility of this element and monatomic material is captured quite accurately in the relation between the nominal ionic compressibility of C [IV] and $Z = 6$ (Figure 6). Then, the $L = 3$ ions Al [VI], Si [IV], Si [VI] are expected to be highly incompressible and this is observed, indeed. Similarly, for $L = 4$, Ge [VI] is the least compressible of the examined ions in this row, etc. Moreover, from Figure 6 one can conclude that the cations of transition group VIIIb elements, the lanthanides, and the actinides should exhibit similar, low-ionic compressibilities. This conclusion is also consistent with experimental observation. Although it is not possible to extract good cation-oxide distances from X-ray diffraction data from high-pressure experiments on compounds of elements with such high form factors, it is known that compounds of $L = 5$ and 6 group VIIIb elements are quite incompressible which, in part, is explained by low cationic compressibility for simple compounds of these elements [81–83].

The relation between $r_0 = C/(Z - S)$ and dr/dP or ionic compressibility β , respectively, explains why pressure-induced changes in outer electron states are correlated to changes in bond coordination rather than inducing an isostructural, continuous evolution of radii

and their compressibilities: C and S are functions of electron states and undergo quantized changes [77–79]. Upon such changes, bond coordination either increases, thereby reducing repulsion, or remains equal, if consistent with Equation (5). Hence, Equation (5) in combination with (2) can be used as a boundary condition for assessing pressure-induced reconstructive transitions. Furthermore, the pressure dependence of the radii is actually not equal to but smaller than $C/(Z - S)$ by the compressibility factor A (Equations (1), (4) and (5)). Factor A therefore represents the relative change of C and S upon compression for a given Z , valence, and coordination, which together with C and S define the radii [77–79]. It is, thus, not surprising the radii r and their dr/dP exhibit some variation around the linear correlation of Equation (1), in consequence of particular settings for S . The effect is seen, for instance, for the dr/dP of Fe^{2+} [VI] which, in high-spin configuration, is somewhat higher than predicted (Figure 6). More generally, radii and dr/dP for a given chemical species but in different coordination are shifted such that in high coordination the distribution of the outer electrons over a more extensive set of configurations reduces repulsion and allows for higher compressibility relative to Equation (1), and coordinations that enhance repulsion give lower dr/dP relative to (1). These variations are equivalent to the positive deviations from the power relation between electronegativity and dr/dP (Figure 6), and Equation (2) can be placed into context with the electron screening functions through $dr/dP = A C/(Z - S) - B = \text{const} \cdot \chi^{-1.76}$. It is important to note that for each chemical species and valence, there is a least one coordination where the radius and dr/dP fall onto the linear correlation of Equation (1) and the power law $dr/dP \sim 1/\chi^{1.76}$ (Equation (2)); thus, these two relations represent the principal trend of ionic compression behaviour.

4.3. General Considerations: Anions

It is proposed that the functional form of $r = r' \cdot P^{-m}$ of the pressure-dependent anions O^{2-} , Cl^- , and Br^- is to be explained in an equivalent fashion: for these anions, $dr/dP = -m \cdot r'/P^{(1+m)} = C'/\{Z - S(P)^{(1+m)}\}$ and the main difference to the cations is in the continuous pressure-dependence of S . In fact, the initial linear anionic compressibilities of O^{2-} , Cl^- , and Br^- fall onto the same correlation of β and Z as the cations (Figure 6, hollow symbols). A quite remarkable aspect in this consistency of cat- and anion compression behaviour is that the initial linear anionic compressibilities of the anions for each row L fall onto the extension of the correlation for $L + 1$ rather than for L , which means that, within the approximation of the crystal radius concept, the initial compression of the anions reflects the full octet state that is formally assigned to them in inorganic chemistry. At large P , the anion radii approach a linear contraction regime like the cations and this change in anion compression regime has been proposed to serve as for a principal distinction of intermediate- and high-pressure phases [5]. The asymptotic high-pressure values also fall into the correlation of β and Z (hollow symbols in Figure 7); however, they are at the tail of the correlations for L rather than on the slopes of the correlation for $L + 1$, close to the singularities of $Z - S$. From a purely formal point of view, this observation implies that within this high-pressure regime O^{2-} [VI], Cl^- [VIII], and Br^- [VIII] have shifted off the octet state. This tentative interpretation is consistent with the proposition by Prewitt and Downs [6] that increasing pressure increases covalency of the bonds. Furthermore, it is consistent with the general pressure-induced reduction of electronegativity [84], which also reduces the difference in electronegativity between cat- and anion, and is therefore in agreement with a reduced electron density gradient along the bond vectors.

If this interpretation holds, the anions exhibit the pressure-induced continuous transition of outer electron states that the cations do not exhibit. There is one observation that indicates pressure-induced changes of electronic configuration that are not directly captured by a configuration at ambient pressure and higher coordination, and that was already noted for Ca in [5]: as mentioned in Section 3 and in Table 2, Ca[VIII] from CsCl-type CaO, Ca[X] from davemaoite, Ba[VIII], and K[VIII] (from B2-type halogenides), interpolate to the ambient pressure crystal radii of Ca[VII, IX], Ba[VII], and K[VI]. However, the radii from compressed lower-pressure compounds of Ca and K with coordinations [VIII] and [X]

interpolate quite exactly to the radii of these coordinations at ambient pressure (obviously, because there is no curvature in the ion compression). This discrepancy is beyond uncertainties and is not result of an erroneous coordination at high pressure (except perhaps for Ba): CaO, KCl, and KBr in the phases have clearly coordination [VIII] and Ca in davemaoite has coordination if at all higher but not lower than [X]. This observation suggests that in some high-pressure compounds, the outer electron configuration of a given ion in a given coordination is different from that at ambient pressure and rather matches that of a lower coordination. However, in contrast to the anions, these possible ‘electronic transitions’ of cations comply with Equation (5) and are between discrete sets of C and S.

4.4. Prediction of Ionic Radii Compression

Based on the systematics that are discussed above, it is possible to predict the pressure derivatives of ionic radii. As mentioned above, for each chemical species and valence, there is a least one coordination where the radius and dr/dP fall onto the linear correlation (1), whereas other coordinations affect the ionic compressibility through their different outer electron configurations, which cause changes in the screening function. The anions are an extreme case of such changes (see Section 4.3). It is tedious and, with the given uncertainties, not necessary to examine the configurations for each of these ions in their different coordinations. Instead, it is found that the separation of two sets of linear correlations between r and dr/dP in Equations (1) and (3) provide sufficient accuracy in predicting the measured dr/dP . This is shown in Figure 7. Only for Li[IV] observed and calculated dr/dP deviate markedly. As indicated above, this deviation is tentatively explained by internuclear repulsion more pronounced than that of heavier ions. Figure 7 also shows that the systematics between dr/dP and Z are predicted to hold for all elements from rows $L = 2$ to 7.

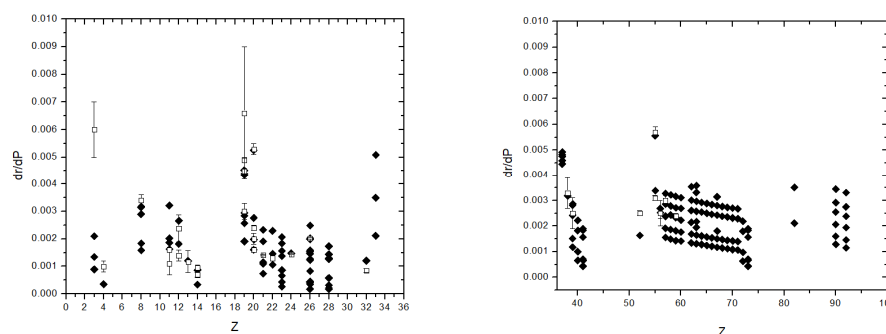


Figure 7. Correlation of pressure dependencies of ionic radii dr/dP in 1/GPa as function of nuclear charge number. Filled diamonds: predicted dr/dP ; hollow squares: observed dr/dP . (**Left panel**): For rows $L = 2$ to 4, (**right panel**): for rows $L = 5$ to 7. For given Z , the different values of dr/dP represent different coordinations. Only Li[IV] deviates markedly and beyond uncertainties from the predicted relation.

5. Summary

In sum, cation compression is negative linear for all 35 examined ions over the examined pressure range. The examined anions exhibit nonlinear compression. The pressure derivative of both cations and anions—are correlated with the nuclear charge number for each row of the periodic table through an inverse relation, modified by a screening function. As for the radii themselves, the screening function depends on the principal and the azimuthal electron states. Consequently, the cationic volume compressibility $(r_0)^{-3} (dr^3/dP)_T$ is nearly invariantly $9.8(1) \cdot 10^{-12} \text{ m}^2/\text{N} = 9.8(1) \cdot 10^{-3} \text{ /GPa}$, which quantifies the change of ionic compressibility with increasing radius, that itself is defined through the addition of further outer electrons for a given principal quantum number L , along with increasing Z , and modified by the screening function S (see Sections 4.2 and 4.3). Therefore, cation compression does generally not result in continuous changes of valence electronic states

but in monotonous linear contraction. Changes in valence electron states appear strictly correlated to changes of bond coordination and are constrained to discrete changes in states that reduce repulsion of the outer electrons. Commonly, changes in bond coordination are achieved through reconstructive phase transitions. For cations, the screening function is not pressure-dependent within uncertainties over the examined pressure range. For anions, the screening function scales with a low power of pressure such that with increasing pressure a linear compression behaviour is approached that is then equivalent to the compression behaviour of the cations. The transition between the initial high compressibility of anions to asymptotic linear compression behaviour at high pressure appears to be a continuous electron transition from a nearly perfect valence electron octet state towards less localized outer electron states, and this appears to define a fundamental difference in anion and cation compression. The more similar compression behaviour at sufficiently high pressure is consistent with the reduced difference in electronegativity between cat- and anion and more shared outer electron states. This behaviour is initially and to first order dominated by the high compressibility of the anions, but in second degree, pressure-induced coordination changes of the cations also modify their electronegativity based on the power-law relation $dr/dP \sim 1/\chi^{1.76}$ that has been established in this paper. Positive and negative excess compressibility of ions in some coordinations is explained as result of lower or higher electron repulsion relative to the coordination-independent electronegativity. These deviations can be quantified in terms of a correction to the electronegativity. The relations between radii, ionic compressibility, electronegativity, and nuclear charge number appear to be general and, thus, allow for predicting pressure dependence of radii for most ions within narrow limits.

The pronounced pressure effect on heavier alkaline and alkaline earth elements, K, Ca, and beyond, is potentially relevant for identifying potential deep mantle signatures in geochemical trace element patterns. In particular, the present results confirm the role of davemaoite as a host of elements that are geochemically incompatible in the upper mantle and, therefore, are compatible in deep mantle rock, where this mineral is stable and operates as solidus phase.

Funding: This research received no external funding.

Data Availability Statement: All data are given in two tables in the paper.

Acknowledgments: The author highly appreciates the thorough reading and insightful comments by the reviewers.

Conflicts of Interest: The author declares no conflict of interest.

References

1. Goldschmidt, V.M. The principles of distribution of chemical elements in minerals and rocks. The seventh Hugo Muller Lecture, delivered before the Chemical Society on 17 March 1937. *J. Chem. Soc.* **1937**, 655–673. [\[CrossRef\]](#)
2. Manjon, F.J.; Errandonea, D.; Lopez-Solano, J.; Rodriguez, P.; Radescu, S.; Mujica, A.; Munoz, A.; Garro, N.; Pellicer-Porres, J.; Segura, A.; et al. Crystal stability and pressure-induced phase transitions in scheelite AWO(4) (A = Ca, Sr, Ba, Pb, Eu) binary oxides. II: Towards a systematic understanding. *Phys. Stat. Sol. B* **2007**, *244*, 295–302. [\[CrossRef\]](#)
3. Li, Z.; Yang, M.J.; Park, J.S.; Wei, S.H.; Berry, J.J.; Zhu, K. Stabilizing Perovskite Structures by Tuning Tolerance Factor: Formation of Formamidinium and Cesium Lead Iodide Solid-State Alloys. *Chem. Mat.* **2016**, *28*, 284–292. [\[CrossRef\]](#)
4. Tschauner, O.; Ma, C. Discovering High-Pressure and High-Temperature Minerals. In *Celebrating the International Year of Mineralogy*; Bindi, L., Cruciani, G., Eds.; Springer: Berlin/Heidelberg, Germany, 2023; pp. 169–206. [\[CrossRef\]](#)
5. Tschauner, O. High-pressure minerals. *Am. Min.* **2019**, *104*, 1701–1731. [\[CrossRef\]](#)
6. Prewitt, C.T.; Downs, R.T. High-pressure crystal chemistry. In *Ultrahigh-Pressure Mineralogy: Physics and Chemistry of the Earth's Deep Interior*; Hemley, R.J., Ed.; Mineralogical Society of America: Washington, DC, USA, 1998; Volume 37, pp. 283–317.
7. Shannon, R.D.; Prewitt, C.T. Coordination and volume changes accompanying high-pressure phase transformations of oxides. *Mat. Res. Bul.* **1969**, *4*, 57–59. [\[CrossRef\]](#)
8. Grochala, W.; Hoffmann, R.; Feng, J.; Ashcroft, N.W. The Chemical Imagination at Work in Very Tight Places. *Angew. Chem. Int. Ed.* **2007**, *46*, 3620–3642. [\[CrossRef\]](#)
9. Gibbs, G.V.; Ross, N.L.; Cox, D.F.; Rosso, K.M.; Iversen, B.B.; Spackman, M.A. Bonded radii and the contraction of the electron density of the oxygen atom by bonded interactions. *J. Phys. Chem. A* **2013**, *117*, 1632–1640. [\[CrossRef\]](#)

10. Gibbs, G.V.; Cox, D.F.; Ross, N.L. The incompressibility of atoms at high pressures. *Am. Min.* **2020**, *105*, 1761–1768. [[CrossRef](#)]
11. Cammi, R.; Rahm, M.; Hoffmann, R.; Ashcroft, N.W. Varying Electronic Configurations in Compressed Atoms: From the Role of the Spatial Extension of Atomic Orbitals to the Change of Electronic Configuration as an Isobaric Transformation. *J. Chem. Theory Comput.* **2020**, *16*, 5047–5056. [[CrossRef](#)]
12. Rahm, M.; Ångqvist, A.; Rahm, J.M.; Erhart, P.; Cammi, R. Non-Bonded Radii of the Atoms Under Compression. *ChemPhys. Chem.* **2020**, *21*, 2441–2453. [[CrossRef](#)]
13. Tschauner, O. An observation related to the pressure dependence of ionic radii. *Geosciences* **2022**, *12*, 246. [[CrossRef](#)]
14. Pauling, L. *The Nature of the Chemical Bond and the Structure of Molecules and Crystals: An Introduction to Modern Structural Chemistry*; Cornell University Press: New York, NY, USA, 1960; p. 644.
15. Shannon, R.D.; Prewitt, C.T. Effective ionic radii in oxides and fluorides. *Acta Crystallogr.* **1969**, *25*, 925–946. [[CrossRef](#)]
16. Shannon, R.D. Revised effective ionic radii and systematic studies of interatomic distances in halides and chalcogenides. *Acta Cryst. A* **1976**, *32*, 751–767. [[CrossRef](#)]
17. Morrison, S.M.; Hazen, R.M. An evolutionary system of mineralogy, Part IV: Planetsimal differentiation and impact mineralization (4566 to 4560 Ma). *Am. Min.* **2021**, *106*, 730–761. [[CrossRef](#)]
18. Du, X.P.; Tse, J.S. Oxygen Packing Fraction and the Structure of Silicon and Germanium Oxide Glasses. *J. Phys. Chem. B* **2017**, *121*, 10726–10732. [[CrossRef](#)]
19. Zhang, J.-M.; Ko, J.-D.; Hazen, R.M.; Prewitt, C.T. High-pressure crystal chemistry of KAlSi₃O₈ hollandite. *Am. Min.* **1993**, *78*, 493–499.
20. Dewaele, A.; Belonoshko, A.B.; Garbarino, G.; Ocellini, F.; Bouvier, P.; Hanfland, M.; Mezouar, M. High-pressure high-temperature equation of state of KCl and KBr. *Phys. Rev. B* **2012**, *85*, 214105. [[CrossRef](#)]
21. Dewaele, A. Equations of State of Simple Solids (Including Pb, NaCl and LiF) Compressed in Helium or Neon in the Mbar Range. *Minerals* **2019**, *9*, 684. [[CrossRef](#)]
22. Dewaele, A. Compression of CsCl and CsBr in the megabar range. *High. Pressure Res.* **2020**, *40*, 402–410. [[CrossRef](#)]
23. Murakami, M.; Hirose, K.; Kawamura, K.; Sata, N.; Ohishi, Y. Post-perovskite phase transition in MgSiO₃. *Science* **2004**, *304*, 855–858. [[CrossRef](#)]
24. Ono, S.; Kikegawa, T.; Ohishi, Y. Equation of state of CaIrO₃-type MgSiO₃ up to 144 GPa. *Am. Min.* **2006**, *91*, 475–478. [[CrossRef](#)]
25. Hazen, R.M.; Finger, L.W. High-pressure and high-temperature crystal-chemistry of beryllium-oxide. *J. All Phys.* **1986**, *59*, 3728–3733. [[CrossRef](#)]
26. Au, Y.; Hazen, R.M. Polyhedral modeling of the elastic properties of corundum and chrysoberyl. *Geophys. Res. Lett.* **1985**, *12*, 725–728. [[CrossRef](#)]
27. Chen, H.; Shim, S.-H.; Leinenweber, K.; Prakapenka, V.; Meng, Y.; Prescher, C. Crystal structure of CaSiO₃ perovskite at 28–62 GPa and 300 K under quasi-hydrostatic stress conditions. *Am. Min.* **2021**, *103*, 462–468. [[CrossRef](#)]
28. Ross, N.L.; Zhao, J.; Angel, R.J. High-pressure single-crystal X-ray diffraction study of YAlO₃ perovskite. *J. Sol. Stat. Chem.* **2004**, *177*, 1276–1284. [[CrossRef](#)]
29. Ross, N. L. High pressure study of Sc Al O₃ perovskite. *Phys. Chem. Min.* **1998**, *25*, 597–602. [[CrossRef](#)]
30. Zhao, J.; Ross, N.L.; Angel, R.J. Polyhedral control of the rhombohedral to cubic phase transition in LaAlO₃ perovskite. *J. Phys. Cond. Matt.* **2004**, *16*, 8763–8773. [[CrossRef](#)]
31. Zhao, J.; Ross, N.L.; Angel, R.J.; Carpenter, M.A.; Howard, C.J.; Pawlak, D.A.; Lukasiewicz, T. High-pressure crystallography of rhombohedral Pr Al O₃ perovskite. *J. Phys. Cond.Matt.* **2009**, *21*, 235403. [[CrossRef](#)] [[PubMed](#)]
32. Ross, N.L.; Zhao, J.; Angel, R.J. High-pressure structural behavior of GdAlO₃ and GdFeO₃ perovskites. *J. Sol. Stat. Chem.* **2009**, *177*, 3768–3775. [[CrossRef](#)]
33. Finger, L.W.; Hazen, R.M. Crystal structure and compression of ruby to 46 kbar. *J. Appl. Phys.* **1978**, *49*, 5823–5826. [[CrossRef](#)]
34. Kim-Zajonz, J.; Werner, S.; Schulz, H. High pressure single crystal X-ray diffraction study on ruby up to 31 GPa. *Z. Krist.* **1999**, *214*, 331–336. [[CrossRef](#)]
35. Lin, J.; Degtyareva, O.; Prewitt, C.T.; Dera, P.; Sata, N.; Gregoryanz, E.; Mao, H.-k.; Hemley, R.J. Crystal structure of a high-pressure/high-temperature phase of alumina by in situ X-ray diffraction. *Nat. Mat.* **2004**, *3*, 389–393. [[CrossRef](#)] [[PubMed](#)]
36. Kantor, A.; Kantor, I.; Merlini, M.; Glazyrin, K.; Prescher, C.; Hanfland, M.; Dubrovinsky, L. High-pressure structural studies of eskolaite by means of single-crystal X-ray diffraction. *Am. Min.* **2012**, *97*, 1764–1770. [[CrossRef](#)]
37. Mao, H.-k.; Shu, J.; Fei, Y.; Hu, J.; Hemley, R.J. The wüstite enigma. *Phys. Earth Planet. Int.* **1996**, *96*, 135–145. [[CrossRef](#)]
38. Yamanaka, T.; Kyono, A.; Nakamoto, Y.; Kharlamova, S.; Struzhkin, V.V.; Gramsch, S.A.; Mao, H.-K.; Hemley, R.J. New structure of high-pressure body-centered orthorhombic Fe₂SiO₄. *Am. Min.* **2015**, *100*, 1736–1743. [[CrossRef](#)]
39. Jacobsen, S.D.; Demouchy, S.; Frost, D.J.; Boffa Ballaran, T.; Kung, J. A systematic study of OH in hydrous wadsleyite from polarized FTIR spectroscopy and single-crystal X-ray diffraction: Oxygen sites for hydrogen storage in earths interior. *Am. Min.* **2005**, *90*, 61–70. [[CrossRef](#)]
40. Hazen, R.M.; Yang, H.X. Effects of cation substitution and order-disorder on P-V-T equations of state of cubic spinels. *Am. Min.* **1999**, *84*, 1956–1960. [[CrossRef](#)]
41. Ma, C.; Tschauner, O.; Beckett, J.R.; Liu, Y.; Rossman, G.R.; Sinogeikin, S.V.; Smith, J.S.; Taylor, L.A. Ahrensite, gamma-Fe₂SiO₄, a new shock-metamorphic mineral from the tissint meteorite: Implications for the tissint shock event on Mars. *Geochim. Cosmochim. Acta* **2016**, *184*, 240–256. [[CrossRef](#)]

42. Yamanaka, T.; Komatsu, Y.; Sugahara, M.; Nagai, T. Structure change of MgSiO₃, MgGeO₃, and MgTiO₃ ilmenites under compression. *Am. Min.* **2005**, *90*, 1301–1307. [[CrossRef](#)]
43. Ross, N.L.; Zhao, J.; Slebochnick, C.; Spencer, E.C.; Chakoumakos, B.C. Petalite under pressure: Elastic behavior and phase stability. *Am. Min.* **2015**, *100*, 714–721. [[CrossRef](#)]
44. Benusa, M.D.; Angel, R.J.; Ross, N.L. Compression of albite, NaAlSi₃O₈. *Am. Min.* **2005**, *90*, 1115–1120. [[CrossRef](#)]
45. Petitgirard, S. Density and structural changes of silicate glasses under high pressure. *High Pressure Res.* **2017**, *37*, 200–213. [[CrossRef](#)]
46. Gatta, G.D.; Angel, R.J.; Zhao, J.; Alvaro, M.; Rotiroli, N.; Carpenter, M.A. Phase stability, elastic behavior, and pressure-induced structural evolution of kalsilite: A ceramic material and high-T/high-P mineral. *Am. Min.* **2011**, *96*, 1363–1372. [[CrossRef](#)]
47. Gatta, G.D.; Lotti, P.; Comboni, D.; Merlini, M.; Vignola, P.; Liermann, H.P. High-pressure behavior of (Cs, K) Al₄Be₅B₁₁O₂₈ (londonite): A single-crystal synchrotron diffraction study up to 26 GPa. *J. Am. Ceram. Soc.* **2017**, *100*, 4893–4901. [[CrossRef](#)]
48. Lazarz, J.D.; Dera, P.; Hu, Y.; Meng, Y.; Bina, C.R.; Jacobsen, S.D. High-pressure phase transitions of clinoenstatite. *Am. Min.* **2019**, *104*, 897–904. [[CrossRef](#)]
49. Finkelstein, G.J.; Dera, P.K.; Jahn, S.; Oganov, A.R.; Holl, C.M.; Meng, Y.; Duffy, T.S. Phase transitions and equation of state of forsterite to 90 GPa from single-crystal X-ray diffraction and molecular modeling. *Am. Min.* **2014**, *99*, 35–43. [[CrossRef](#)]
50. Ross, N.L.; Hazen, R.M. High-pressure crystal chemistry of Mg Si O₃ perovskite. *Phys. Chem. Min.* **1990**, *17*, 228–237. [[CrossRef](#)]
51. Kudoh, Y.; Ito, E.; Takeda, H. Effect of pressure on the crystal structure of perovskite type Mg Si O₃. *Phys. Chem. Min.* **1987**, *14*, 350–354. [[CrossRef](#)]
52. Sugahara, M.; Yoshiasa, A.; Komatsu, Y.; Yamanaka, T.; Bolfan Casanova, N.; Nakatsuka, A.; Sasaki, S.; Tanaka, M. Reinvestigation of the MgSiO₃ perovskite structure at high pressure. *Am. Min.* **2006**, *91*, 533–536. [[CrossRef](#)]
53. Richet, P.; Mao, H.-K.; Bell, P.M. Static compression and equation of state of CaO to 1.35 Mbar. *J. Geophys. Res.* **1988**, *93*, 15279–15288. [[CrossRef](#)]
54. Zhao, J.; Ross, N.L.; Wang, D.; Angel, R.J. High-pressure crystal structure of elastically isotropic CaTiO₃ perovskite under hydrostatic and non-hydrostatic conditions. *J. Phys. Cond. Matt.* **2011**, *23*, 455401. [[CrossRef](#)] [[PubMed](#)]
55. Milani, S.; Comboni, D.; Lotti, P.; Fumagalli, P.; Ziberna, L.; Maurice, J.; Hanfland, M.; Merlini, M. Crystal structure evolution of CaSiO₃ polymorphs at earth's mantle pressures. *Minerals* **2021**, *11*, 652. [[CrossRef](#)]
56. Xiao, W.; Tan, D.; Zhou, W.; Liu, J.; Xu, J. Cubic perovskite polymorph of strontium metasilicate at high pressures. *Am. Min.* **2013**, *98*, 2096–2104. [[CrossRef](#)]
57. Loridant, S.; Lucazeau, G.; Le Bihan, T. A high-pressure Raman and X-ray diffraction study of the perovskite SrCeO₃. *J. Phys. Chem. Sol.* **2002**, *63*, 1983–1992. [[CrossRef](#)]
58. Knight, K.S.; Marshall, W.G.; Bonanos, N.; Francis, D.J. Pressure dependence of the crystal structure of SrCeO₃ perovskite. *J. All Comp.* **2005**, *394*, 131–137. [[CrossRef](#)]
59. Errandonea, D.; Kumar, R.S.; Ma, X.; Tu, C. High-pressure X-ray diffraction of SrMoO₄ and pressure-induced structural changes. *J. Sol. Stat. Chem.* **2008**, *181*, 355–364. [[CrossRef](#)]
60. Crichton, W.; Merlini, M.; Hanfland, M.; Mueller, H. The crystal structure of barite, Ba(SO₄), at high pressure. *Am. Min.* **2011**, *96*, 364–367. [[CrossRef](#)]
61. Santamaria-Perez, D.; Chulia-Jordan, R. Compression of mineral barite, BaSO₄: A structural study. *High. Pressure Res.* **2012**, *32*, 81–88. [[CrossRef](#)]
62. Errandonea, D.; Pellicer-Porres, J.; Manjón, F.J.; Segura, A.; Ferrer-Roca, C.; Kumar, R.S.; Tschauner, O.; López-Solano, J.; Rodríguez-Hernández, P.; Radescu, S.; et al. Determination of the high-pressure crystal structure of BaWO₄ and PbWO₄. *Phys. Rev. B Cond. Matt. Mat. Phys.* **2006**, *73*, 224103. [[CrossRef](#)]
63. Yusa, H.; Sata, N.; Ohishi, Y. Rhombohedral(9R) and hexagonal(6H) perovskites in barium silicates under high pressure. *Am. Min.* **2007**, *92*, 648–654. [[CrossRef](#)]
64. Friedrich, A.; Kunz, M.; Miletich, R.; Pattison, P. High-pressure behavior of Ba(OH)₂: Phase transitions and bulk modulus. *Phys. Rev. B Cond. Matt. Mat. Phys.* **2002**, *66*, 214103. [[CrossRef](#)]
65. Hayward, S.A.; Redfern, S.A.T.; Stone, H.J.; Tucker, M.G.; Whittle, K.R.; Marshall, W.G. Phase transitions in BaTiO₃: A high-pressure neutron diffraction study. *Z. Krist.* **2005**, *220*, 735–739. [[CrossRef](#)]
66. Hazen, R.M.; Finger, L.W.; Hemley, R.J.; Mao, H.K. High-pressure crystal chemistry and amorphization of alpha quartz. *Solid State Commun.* **1989**, *72*, 507–511. [[CrossRef](#)]
67. Levien, L.; Prewitt, C.T.; Weidner, D.J. Structure and elastic properties of quartz at pressure. *Am. Min.* **1980**, *65*, 920–930.
68. Angel, R.J.; Shaw, C.S.J.; Gibbs, G.V. Compression mechanisms of coesite. *Phys. Chem. Min.* **2003**, *30*, 167–176. [[CrossRef](#)]
69. Kudoh, Y.; Takeda, H. Single crystal X-ray diffraction study on the bond compressibility of fayalite, Fe₂SiO₄ and rutile, TiO₂ under high pressure. *Phys. B + C Phys. Cond. Matt.* **1986**, *139*, 333–336. [[CrossRef](#)]
70. Andraut, D.; Angel, R.J.; Mosenfelder, J.L.; Le Bihan, T. Equation of state of stishovite to lower mantle pressures. *Am. Min.* **2003**, *88*, 301–307. [[CrossRef](#)]
71. Zhang, L.; Popov, D.; Meng, Y.; Wang, J.; Ji, C.; Li, B.; Mao, H.K. In-situ crystal structure determination of seifertite SiO₂ at 129 GPa: Studying a minor phase near Earth's core-mantle boundary. *Am. Min.* **2016**, *101*, 231–234. [[CrossRef](#)]
72. Ross, N.L.; Shu, J.-F.; Hazen, R.M.; Gasparik, T. High-pressure crystal chemistry of stishovite. *Am. Min.* **1990**, *75*, 739–747.

73. Yamanaka, T.; Fukuda, T.; Tsuchiya, J. Bonding character of SiO₂ stishovite under high pressures up to 30 GPa. *Phys. Chem. Min.* **2002**, *29*, 633–641. [[CrossRef](#)]
74. Sugiyama, M.; Endo, S.; Koto, K. The crystal structure of stishovite under pressure up to 6 GPa. *Miner. J.* **1987**, *13*, 455–466. [[CrossRef](#)]
75. Tschauner, O.; Huang, S.; Yang, S.; Humayun, M.; Liu, W.; Gilbert Corder, S.N.; Bechtel, H.A.; Tischler, J.; Rossmann, G.R. Discovery of davemaoite, CaSiO₃-perovskite, as a mineral from the lower mantle. *Science* **2021**, *374*, 891–894.
76. Rahm, M.; Zeng, T.; Hoffmann, R. Electronegativity Seen as the Ground-State Average Valence Electron Binding Energy. *J. Am. Chem. Soc.* **2019**, *141*, 342–351. [[CrossRef](#)] [[PubMed](#)]
77. Pauling, L. The theoretical prediction of the physical properties of many-electron atoms and ions. *Proc. Roy. Acad. Ser. A* **1927**, *114*, 181–211.
78. Slater, J.C. Atomic Shielding Constants. *Phys. Rev.* **1930**, *36*, 57–64. [[CrossRef](#)]
79. Clementi, E.; Raimondi, D.L. Atomic Screening Constants from SCF Functions. *J. Chem. Phys.* **1963**, *38*, 2686–2689. [[CrossRef](#)]
80. Gillet, P.; Fiquet, G.; Daniel, I.; Reynard, B.; Hanfland, M. Equations of state of 12C and 13C diamond. *Phys. Rev. B* **1999**, *60*, 14660–14664. [[CrossRef](#)]
81. Crowhurst, J.C.; Goncharov, A.F.; Sadigh, B.; Evans, C.L.; Morrall, P.G.; Ferreira, J.L.; Nelson, A.J. Synthesis and characterization of the nitrides of platinum and iridium. *Science* **2006**, *311*, 1275–1278. [[CrossRef](#)]
82. Haines, J.; Leger, J. Phase-transitions in ruthenium dioxide up to 40 GPa—Mechanism for the rutile-to-fluorite phase-transformation and a model for the high-pressure behavior of stishovite SiO₂. *Phys. Rev. B* **1993**, *48*, 13344–13350. [[CrossRef](#)]
83. Tschauner, O.; Kiefer, B.; Tetard, F.; Tait, K.; Bourguille, J.; Zerr, A.; Dera, P.; McDowell, A.; Knight, J.; Clark, C. Elastic moduli and hardness of highly incompressible platinum perpnictide PtAs₂. *Appl. Phys. Lett.* **2013**, *103*, 101901. [[CrossRef](#)]
84. Rahm, M.; Cammi, R.; Ashcroft, N.W.; Hoffmann, R. Squeezing All Elements in the Periodic Table: Electron Configuration and Electronegativity of the Atoms under Compression. *J. Am. Chem. Soc.* **2019**, *141*, 10253–10271. [[CrossRef](#)]

Disclaimer/Publisher's Note: The statements, opinions and data contained in all publications are solely those of the individual author(s) and contributor(s) and not of MDPI and/or the editor(s). MDPI and/or the editor(s) disclaim responsibility for any injury to people or property resulting from any ideas, methods, instructions or products referred to in the content.